Guided-Wave Acoustooptic Interaction with Phase Modulation in a ZnO Thin-Film Transducer on an Si-Based Integrated Mach–Zehnder Interferometer

E. Bonnotte, Christophe Gorecki, Hiroshi Toshiyoshi, H. Kawakatsu, H. Fujita, Kerstin Wörhoff, and K. Hashimoto

***Abstract*— This paper presents the design and the realization of a novel integrated Mach–Zehnder interferometer (MZI) with heterodyne schema. Well-controlled machining as well as ZnO thin-film transducer integration on the same Si substrate permits to transform an optically passive device to an active device with sinusoidal phase modulation. Theoretical and experimental results are presented, demonstrating that an efficient sensor can be designed and fabricated.**

***Index Terms*— Acoustooptic modulation, micro-opto-electro-mechanical systems (MOEMS), optical interferometry, optical strip waveguides, surface acoustic waves.**

I. Introduction

THE combination of integrated optics and micromechanical structures on silicon creates a new class of microopto-electromechanical (MOEM) devices and offers new integration potentials for sensing applications. Fabrication of microstructures using batch processes has a lot of following advantages: low cost, availability in large size, good mechanical behavior, possibility to hybridize or integrate laser diodes and detectors directly on the substrate, efficient coupling between optical fibers and silicon-based waveguide, and possible association on the same chip with other optical components (lenses, beamsplitters) and micromechanics (membranes, beams) [1], [2]. It is also possible to build phase modulators by using microstructures that interact with the guided light by altering the refractive index of the guiding region. Three main physical effects used to generate a phase modulation in thin-film optical waveguides are electrooptic, thermooptic, and acoustooptic, respectively [3]. These modulators consist of a dielectric waveguide and an appropriate electrode structure. The device structure can be classified into two generic categories: 1) the substrate on which the optical waveguide is constructed is a piezoelectric material and 2) the substrate is a nonpiezoelectric material [4]. The linear electrooptic effect, which allows operation in the first category, offers efficient modulation up to a 10 GHz frequency range. It is restricted to piezoelectric substrates like as $LiNbO_3$, $LiTaO_3$, or GaAs with large Pockels coefficients. In terms of physical characteristics required to generate of high efficient phase modulation, one concludes that $LiNbO_3$ is the best material. However, the choice of a substrate material is not only based on its physical features. Since MOEM's are mainly constructed on substrates with silicon-based layers, it is attractive to fabricate modulators on nonpiezoelectric substrates. Thermooptic and acoustooptic allow in principle operation in this category, but thermooptic modulators are limited to a kilohertz range. Acoustooptic using surface acoustic waves (SAW's), which is proposed here, can be used for modulators in a megahertz range. To obtain a device under active phase modulation, a SAW will be generated by means of a thin-film piezoelectric transducer deposited near the silicon-based optical waveguide. acoustooptic interaction mechanism is then based on the change in the index of refraction caused by mechanical strain which is introduced by the passage of an acoustic wave [5], [6]. An optical spectrum analyzer using this modulation technique has been reported, working up to a 1 GHz frequency range [7].

Manuscript received May 1, 1998; revised October 7, 1998. This work was supported by the Canon Foundation in Europe.

E. Bonnotte, H. Toshiyoshi, H. Kawakatsu, and H. Fujita are with the LIMMS/CNRS, Institute of Industrial Science, University of Tokyo, Tokyo 106-8558 Japan.

C. Gorecki was with the LIMMS/CNRS, Institute of Industrial Science, University of Tokyo, Tokyo 106-8558 Japan. He is now with Laboratoire d'Optique P.M. Duffieux, Faculté des Sciences, Université de Franche-Comté, Besançon 25030 France.

K. Wörhoff is with MESA—the Department of Applied Physics, University of Twente, 7500 Enschende, The Netherlands.

K. Hashimoto is with the Faculty of Engineering, University of Chiba, Chiba-shi, Japan.

Publisher Item Identifier S 0733-8724(99)00519-8.

II. Design of Integrated Architecture

The proposed Mach–Zehnder interferometer (MZI) architecture is shown in Fig. 1 [8].

It consists of combining measurement and reference arms of the interferometer composed of two symmetrical Y-junctions integrated on a silicon substrate. Phase modulation is obtained by passing the guided reference beam through a SAW generated on a ZnO thin-film transducer driven by an interdigital electrode structure. ZnO has a low dielectric constant and a high electromechanical coupling factor making this an interesting material for SAW devices. To avoid perturbations on the measuring arm of the interferometer, acoustic waves have to be confined to the region of the reference arm by means of an isolation trench. This isolation trench is filled with an acoustic absorber.

A. Optical Waveguide

For our specific application a single-mode silicon oxinitride (SiO_xN_y) strip-loaded waveguide is preferred (Fig. 2),

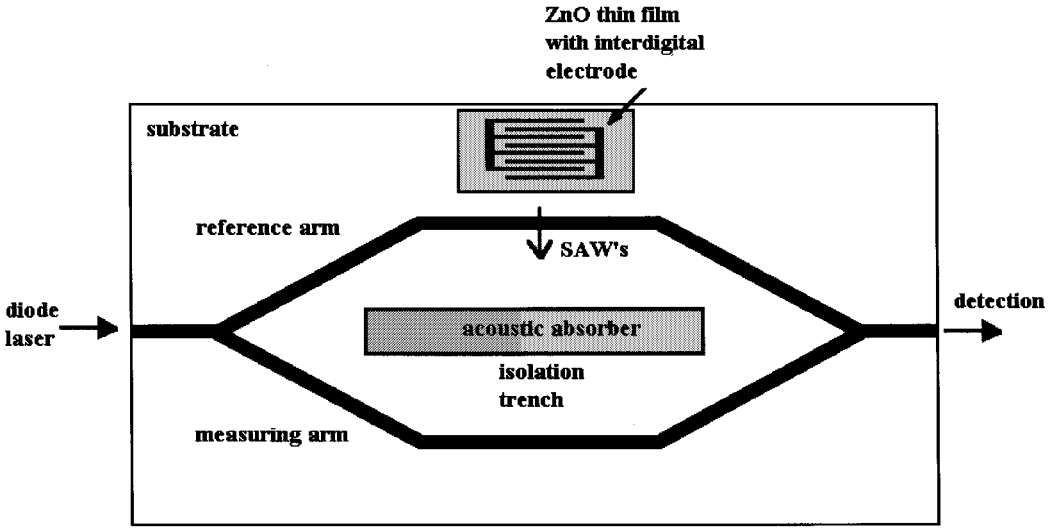

Fig. 1. Schematic diagram of the integrated Mach–Zehnder interferometer with phase modulation.

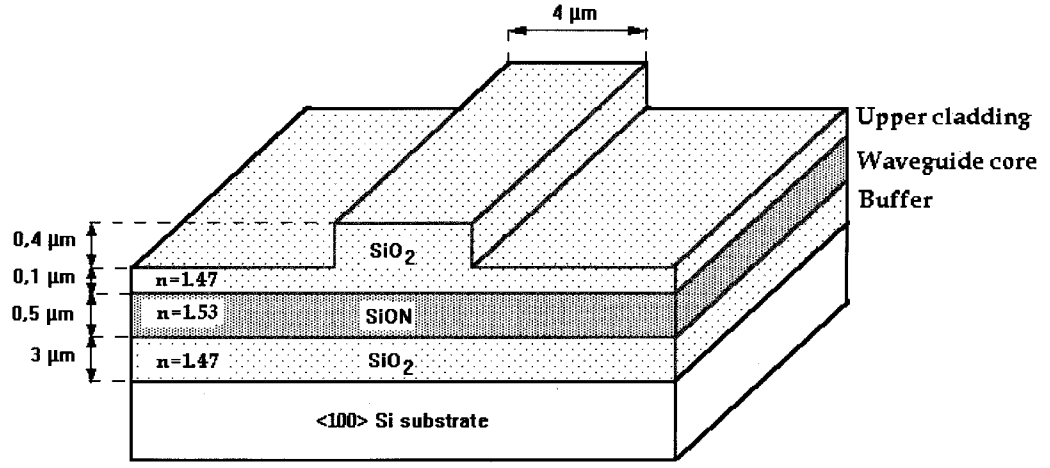

Fig. 2. Cross section of the optical single-mode strip-loaded waveguide operated at 633 nm wavelength.

operating at 633 nm wavelength. The waveguide core is a SiO_xN_y thin film of 0.5 μm with a refractive index $n = 1.53$, sandwiched between two SiO_2 cladding layers with refractive indexes $n = 1.47$. A 4-μm wide rib is etched in the SiO_2 upper cladding layer. This overlayer structure laterally confines the optical field.

Fig. 3 shows the calculated field distribution of a single-mode $SiO_2/SiO_xN_y/SiO_2$ strip-loaded waveguide operating at 633 nm wavelength. This calculation were performed with a two-dimensional (2-D) mode solver software using the effective index method. This confirms an excellent confinement of the optical field for the previously described structure and permits visualization of the lateral size of the guided TE_{00} mode. The waveguide is single-mode up to 4.5–5 μm waveguide width. Fig. 4 illustrates the propagation of optical field along one Y-junction of 12 mm total length with a gap of 400 μm between both the branches. This calculation were performed for TE polarization using three-dimensional (3-D) beam propagation method (BPM). To decrease the losses in the Y-junction, the curvatures are of S-bend type based on a cosine function, where the curvature of minimum radius is used to connect the start and end coordinates.

B. Thin-Film Piezoelectric Transducer

The elastooptic is generated by the strain due to the presence of an acoustic wave which causes a change in the tensor components of the dielectric permeability $\mathbf{B}$ [9]. This requires a tensor relation between the elastic strain and the elastooptic coefficient

$$\Delta B_{ij} = p_{ijkl} S_{kl} \qquad i, j, k, l = 1, 2, 3 \tag{1}$$

where p_{ijkl} is a fourth-rank elastooptic tensor, and S_{kl} are the strain components.

The elastic strain produces a grating-shaped variation of the index of refraction within the waveguide. The resulting index variation is periodic, with a wavelength equal to that of the

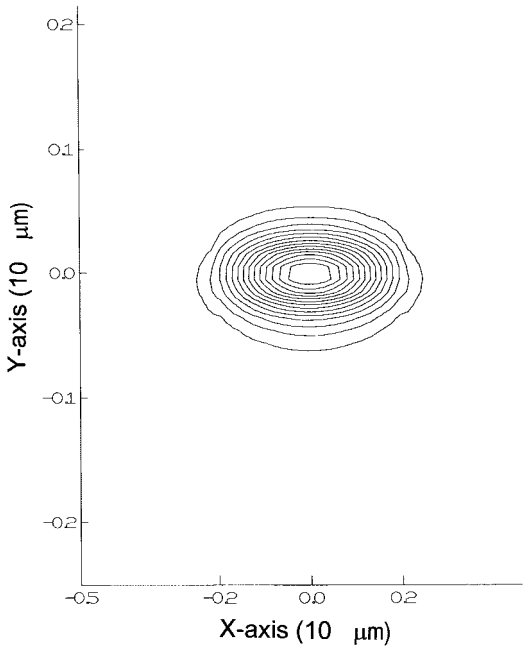

Fig. 3. Optical field distribution in the cross section of a single-mode strip-loaded waveguide calculated by the effective index method.

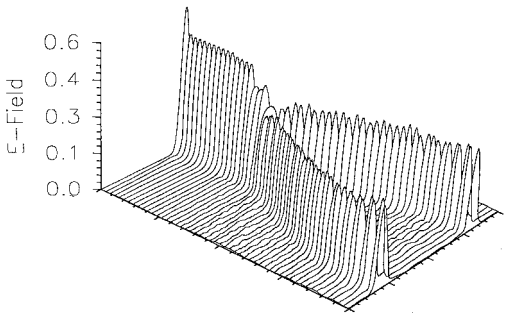

Fig. 4. Optical field distribution of a 12-mm long Y-junction with a gap of 400 μm between the branches, calculated by BPM.

acoustic wave. The period of the grating is

$$\Lambda = \frac{v_a}{f_c} \tag{2}$$

where f_c is the acoustic frequency, and v_a the velocity of SAW's. The change in the index of refraction n_{ij} is

$$\Delta n_{ij} = -\tfrac{1}{2}\, n_{ij}^3 p_{ijkl} S_{kl} \qquad i, j, k, l = 1, 2, 3. \tag{3}$$

Assuming the medium isotropic, in order to avoid the tensor notation, (3) becomes

$$\Delta n = -\tfrac{1}{2}\, n^3 p S. \tag{4}$$

When a sinusoidal SAW propagates along the x-axis, the refractive index in the region of the acoustooptic interaction is

$$n(x, t) = n + \Delta n \sin(\Omega t + Kx) \tag{5}$$

where $K = 2\pi/\Lambda$ is the wave number, n is the average refractive index of the medium, and Ω is the frequency of SAW.

We calculated numerically the elastic strain distribution using the ANSYS[1] software performing a finite element simulation. Material properties required by the simulation tool are the three matrices characterizing the piezoelectric element (piezoelectric, elastic coefficients, and permitivity). Rotations are applied to the matrices to take into account that we have to generate SAW's and so, ZnO c-axis were adjusted perpendicularly to the substrate plane. The piezoelectric transducer model is shown in Fig. 5(a), where a voltage of 100 V is applied to four interdigital electrodes. For the geometry considered the strain S distribution is shown in Fig. 5(b), where the maximum amplitude of strain is around 0.87×10^{-4} N/m^2. The elastooptic coefficient $p = 0.27$ of silica is very similar to those of the waveguide plasma-enhanced chemical vapor deposition (PECVD) layers. Consequently, the maximum amplitude of refractive index change due to the acoustic strain is approximately $\Delta n = 0.5 \times 10^{-4}$.

III. Fabrication Technology

Fig. 6 illustrates main fabrication sequences of Mach–Zehnder integrated interferometer.

The devices have been realized on $\langle 100 \rangle$ oriented 3 in silicon wafer. The planar optical waveguide consisting of an SiO_2–SiO_xN_y–SiO_2 layer stack have been deposited by PECVD. The schematic diagram of the used parallel plate Electrotech Plasmafab 310 PECVD reactor is shown in Fig. 7. In this configuration, the frequency of the power generator is 187.5 kHz. SiO_xN_y and SiO_2 layers are deposited at a plasma power of 60 W, a chamber pressure of 650 mTorr and a lower platen temperature of 300 °C. The refractive indexes of the layers to be deposited is tuned by changing the ratio between the processing gases, 2% SiH_4 diluted in N_2, N_2O, and NH_3, as shown in Fig. 8. For the realization of the waveguiding structure, the lower and upper cladding layers (PECVD SiO_2) have been deposited with 200 sccm of 2% SiH_4/N_2 and 710 sccm N_2O, resulting in thin film with a refractive index of 1.47. The silicon oxynitride core layer, having a refractive index of 1.53, has been grown applying 1000 sccm 2% SiH_4/N_2, 900 sccm N_2O, and 6 sccm NH_3. In the upper SiO_2 cladding a 4-μm wide rib is structured with a resist mask in a reactive ion etching (RIE) process using CHF_3 plasma. The obtained etch rate is 30 nm/min. To pattern the isolation trench a deep RIE etching using a mixture of $He/SF_6/O_2$ gases is performed. To pattern the interdigital electrode of the piezoelectric transducer a thin film of Cr was deposited by vacuum evaporation on the front surface of the wafer. The metal layer is subsequently wet etched to pattern the transducer electrode. The distance between the electrode system and the waveguide is 0.3 mm. The deposition condition to generate SAW's is obtained when the c-axis of the ZnO-layer is perpendicular to the substrate. ZnO thin film is deposited by sputtering directly on the top of the SiO_2 upper

[1] ANSYS is a registered trademark of ANSYS Incorporated.

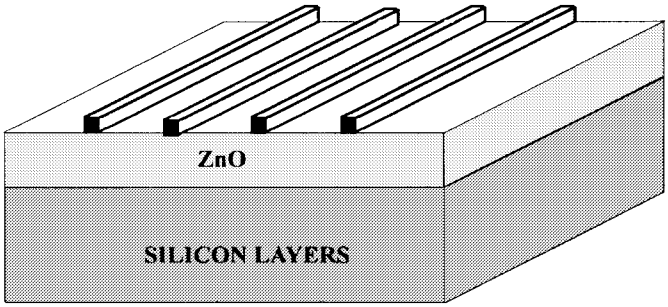

(a)

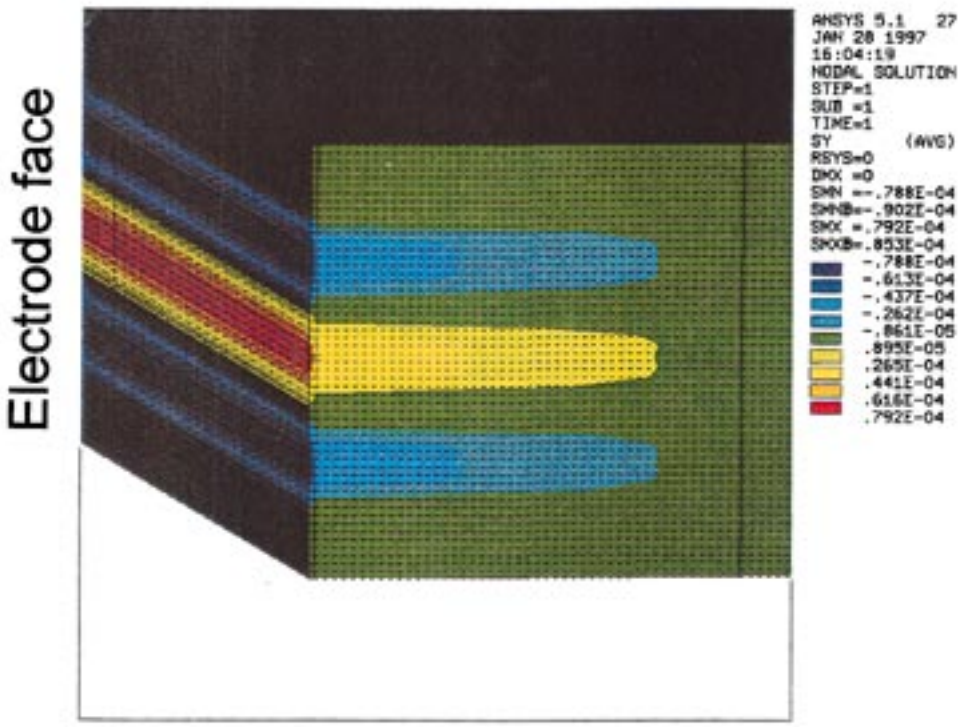

(b)

Fig. 5. ANSYS simulation of strains: (a) ZnO thin-film transducer model with four electrodes and (b) strain distribution along the direction perpendicular to electrodes.

cladding near the reference arm of the interferometer. A 3 μm thick ZnO film is fabricated by the target facing sputtering method (TFSM) which holds two symmetrical targets of pure zinc. In this modified sputtering system, the substrate on which the ZnO to be deposited is suspended perpendicular between the targets, as seen in Fig. 9, so a very strong confinement of plasma is obtained. The sputtering deposition were made in pure oxygen atmosphere at 150 °C temperature and in 7 mTorr gas pressure. The deposition rate of 0.5 μm/h and the ZnO film resistivity about 10^9 Ω.cm are obtained. In the last fabrication sequence the ZnO layer is removed outside the piezoelectric transducer area.

Fig. 10(a) represents a SEM photograph of one of Y-junctions just after the patterning of the SiO_2 rib by RIE. Fig. 10(b) shows the structure of the transducer interdigital electrode with 15 fingers, where the connection is gold wire bonded.

IV. Experimental Performances

To evaluate the optical performance, a He–Ne laser beam operating at 633 nm is coupled into the waveguide via a microscope objective lens. The strip-load waveguide loss measured by a cut-back technique was 0.5 dB/cm for TE_0 polarization. In this wavelength range the optical loss is lower than at 780 nm wavelength, resulting from lower absorption of evanescent field on the silicon substrate. The size of the TE_{00} guided mode was estimated to be about 4.5 μm (Fig. 3), and it was much smaller than the SAW wavelength of 60 μm. In this condition there will be no diffraction and the guided optical wave will only be sinusoidal phase modulated. Phase modulation experiment is conducted by detecting the spectrum of the interference signal via a spectral analyzer, as shown in Fig. 11. It was obtained at SAW drive power of $P_a = 11$ mW (P_a is the acoustic power over the interaction

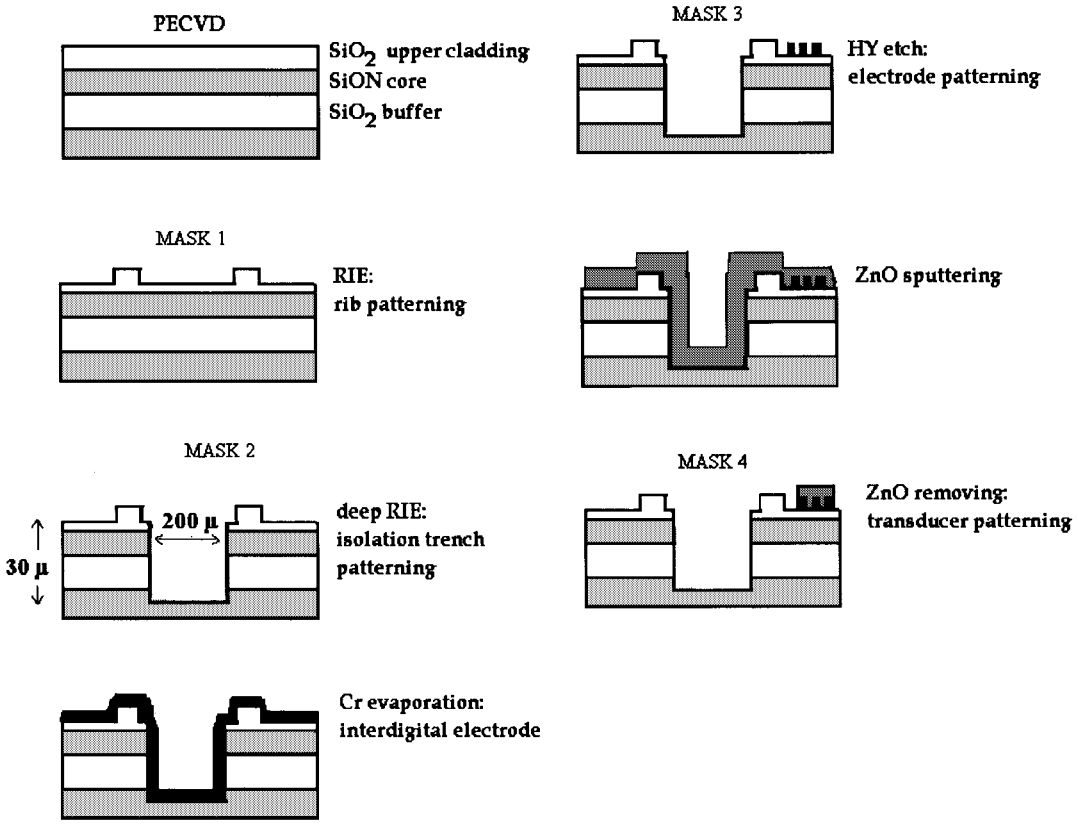

Fig. 6. Fabrication sequences of the integrated Mach–Zehnder interferometer with phase modulation.

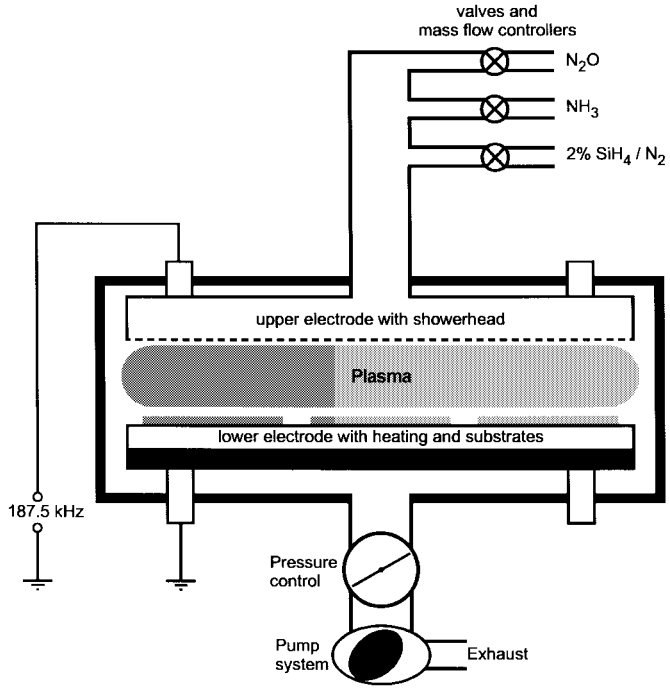

Fig. 7. Schematic diagram of the parallel plate PECVD reactor.

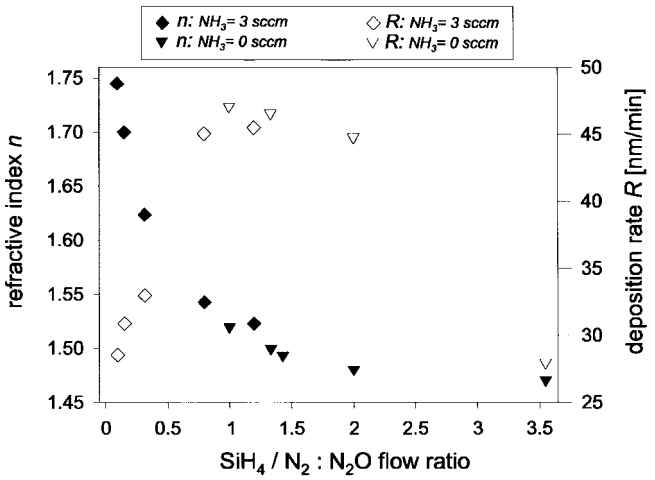

Fig. 8. Refractive index and deposition rate of PECVD film growth at varied processing gas ratio.

width $L = 5.8$ mm). As expected, there was a component corresponding to the SAW frequency $f_0 = 48$ MHz (first harmonic). The second and third harmonics also appeared as frequency components spaced by f_0. From the detected ratio of the first to third harmonics it was possible to estimate the phase shift. The amplitude of the third harmonic was about $20 \log[J_1(\delta\varphi)/J_3(\delta\varphi)] = 22$ dB below the first harmonic, where $J_i\,(i = 1, 3)$ are the Bessel functions. Accordingly this $J_1(\delta\varphi)/J_3(\delta\varphi) = 12.7$, and the phase shift was determined to be $\delta\varphi = 1.3$ rad.

Several figures of merit have been used to characterize the phase modulator: electromechanical coupling efficiency, bandwidth characteristics, and isolation between both the interferometer arms.

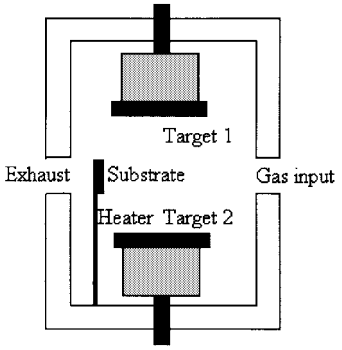

Fig. 9. Geometry for sputtering substrate/targets assembly.

1) Electromechanical Coupling Efficiency: For a N-period interdigital transducer, the frequency variation of acoustic amplitude can be approximated for frequencies near ω_0 by the function $\sin x/x$ where $x = N\pi(\omega - \omega_0)/\omega_0$. The useful criterion of transducer performance is the transducer quality factor defined as [10], [11]

$$\frac{1}{Q} = \omega_0 N C_S R_A = N\pi \frac{\Delta v}{v} = \frac{\pi}{2} N k^2 \tag{6}$$

with $k^2 = 2(\Delta v/v)$, where ω_0 is the center frequency of the frequency bandwidth, C_s is the elementary finger capacitance, k^2 is the electromechanical coupling coefficient, R_A is the radiation impedance, and Δv is the change in acoustic velocity caused by introducing a short-circuiting plane in the plane of interdigital electrode. The effect of Δv change can be simulated numerically by metallizing of ZnO film/silicon interface.

The theoretical electromechanical coupling efficiency of a thin-film transducer vary with ZnO film thickness. This thickness dependence is shown theoretically in Fig. 12. For a ZnO thin film of 3 μm thick the theoretical value of electromechanical coupling coefficient is $k^2 = 0.0025$. The experimentally measured electromechanical coupling coefficient reach a maximum value near 0.0019. This is 77% that of theoretical value. The experimental k^2 value were calculated from conversion loss measurements in the next section.

2) Bandwidth Characteristics: Under the condition of the matching network defined in [10] the electronic bandwidth of the system is determined by the product $\Delta v/v$ and the number N of finger pairs. Q is then proportional to $1/N$ when the optimum value of N is used. Our transducer has an interdigital period of 60 μm (this corresponds to a frequency of $f_0 = 48$ MHz) with a finger width of 15 μm and an electrode aperture width of $L = 5.8$ mm. When $R_A = 75\ \Omega$, and $C_s = 0.14$ pF, the transducer with $N = 15$ was found to have the optimum fractional bandwidth of 0.08, corresponding to a 3 dB conversion loss ($1/N$ was 0.067). We evaluated the bandwidth characteristics of the transducer by measuring the conversion loss of a delay line (Fig. 13). This delay line was composed from two identical interdigital electrodes placed one after other with the spacing between the input and output transducers of 7 mm, giving a delay of approximately 2.2 μs. This was connected to a source generator with an impedance of 50 Ω. Fig. 14 shows, respectively, a comparison of calculated and measured conversion losses for this delay line plotted as a function of frequency for a 3 μm ZnO film. The conversion loss is defined as $CL = 10\log(P_S/P_{IN})$ where P_S is the maximum power available from the generator source, and P_{IN} is the power absorbed inside the delay line. In practice, the measuring procedure consisted of detecting power variations between two transducers. As we can see there is a good agreement between the experimental and theoretical responses. The transducer centered at 48 MHz have 3-dB wideband value of 5 MHz corresponding to the conversion loss of about 2.8 dB.

3) Isolation: The isolation describes the optical intensity appearing through the measuring arm of the interferometer. An isolation of about 22 dB were measured experimentally. The attenuation of absorption is due to the using of an acoustic absorber (Araldite glue).

V. Conclusion and Perspectives

We have realized a silicon-based microinterferometer with significant SAW phase modulation, performed by deposition of a ZnO thin-film transducer. The key reason for choosing a silicon-based multilayer waveguide is that this structure provides a flexible tool for designing of the best optical architecture needed to increase the efficiency of acoustooptic interactions. In addition, this is interesting in view of the compatibility with MEMS technology.

The future biomedicine application of the device will be *in situ* optical monitoring of the capillary-alveolar barrier [12]. An increase of this permeability is a signal which determines inflammations of lung or abnormalities of respiratory organs of adults. The estimation of the permeability is made actually by measuring the passage of a fluorescent macromolecule indicator from the vascular to the alveolar compartment. Measurements can be performed directly by evaluation the concentration of the fluorescent indicator inside the free air of the lung. To monitor the permeability, a probe is introduced to take a sample and to analyze it in the laboratory. It is a long, expensive, and invasive technique. To improve this standard technique we propose the combination of the fluorescent indicator with a measuring unit such as the proposed integrated Mach–Zehnder interferometer. The miniaturization of the sensor should allow it to be inserted through the operating canal of the bronchoscope with the follows benefits: i) continuous measurement of fluorescence and ii) measurement of fluorescence in small airways inaccessible to a standard bronchoscope. For this application the measuring arm of Mach–Zehnder interferometer will be covered with a polymer layer, sensitive to liquid compounds to be measured, modifying the effective index of refraction of the structure. The working principle is the follows: the fluorescent liquid to be measured is absorbed by the sensitive polymer film, which change its refractive index with the absorption amount. As the intensity distribution of waveguided modes is not totally confined to the wave-

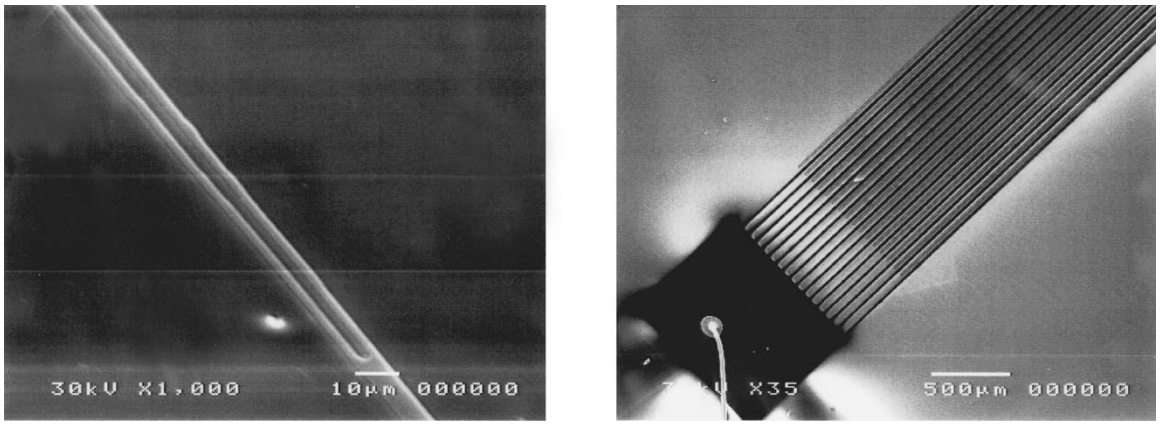

(a) (b)

Fig. 10. SEM photographs of structures: (a) Y-junction with a 4-μm rib after RIE and (b) Cr interdigital electrode with gold wire bonded connection.

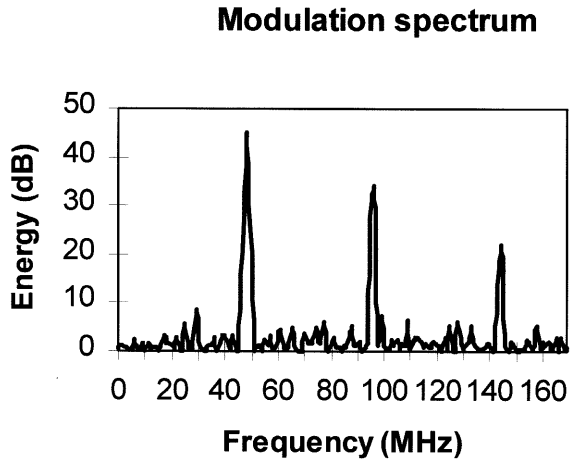

Fig. 11. Measured modulation spectrum using a SAW power of 11 mW.

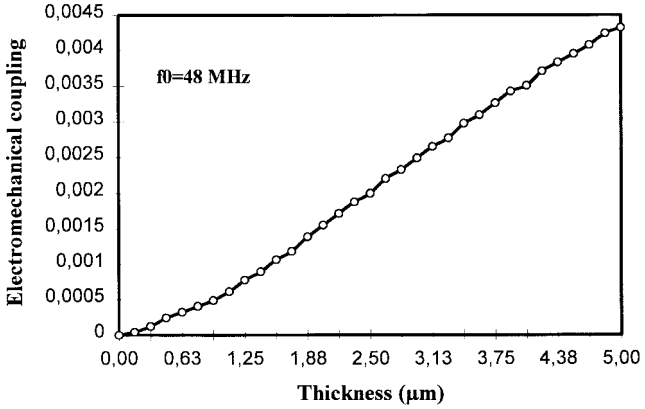

Fig. 12. Theoretical dependence of the electromechanical coupling coefficient on the ZnO film thickness.

guide, the interferometer phase changes with the refractive index of the polymer film. The output intensity will be modulated as a function of the concentration of fluorescent indicator, resulting in phase shift of interference fringes. With a measuring window of 10 mm long, the measuring of effective refractive index changes as small as 10^{-5} is

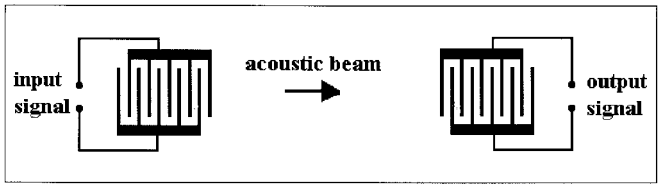

Fig. 13. Schematic diagram of the delay line.

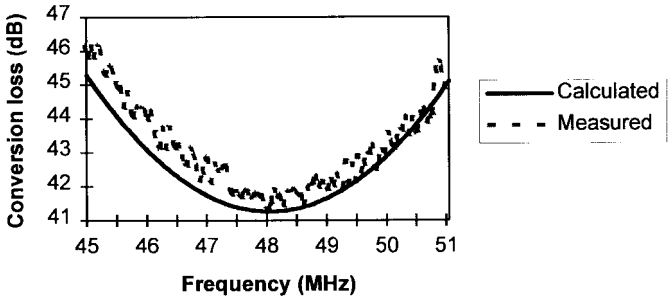

Fig. 14. Comparison of theoretical and measured conversion losses for a delay line with 15 finger pair transducer.

expected, corresponding to fluorescence concentration down to 10 ppm.

ACKNOWLEDGMENT

The authors wish to thank P. Linders for help in deposition of PECVD layers.

REFERENCES

[1] D. Peters, K. Fisher, and J. Müller, "Integrated optics based on silicon oxinitride thin films deposited on silicon substrates for sensor applications," *Sensors Actuators*, vol. A, no. 25–27, pp. 425–431, 1991.
[2] H. Bezzaoui and E. Voges, "Integrated optics combined with micromechanics on silicon," *Sensors Actuators*, vol. A, no. 29, pp. 219–223, 1991.
[3] R. G. Hunsperger, *Integrated Optics: Theory and Technology.* Berlin, Germany: Springer Verlag, 1991, p. 124.
[4] C. H. Von Helmolt, "Integrated optics strip waveguide phase modulator driven by a SAW," *J. Lightwave Technol.*, vol. LT-5, pp. 218–228, Feb. 1987.
[5] C. P. Sandbank and M. B. N. Butler, "Acoustic surface waves on isopaustic glass," *Electron. Lett.*, vol. 7, no. 7, pp. 499–501, 1971.

[6] F. S. Hickernell, "DC triode sputtered zinc oxide surface elastic wave transducers," *J. Appl. Phys.*, vol. 44, no. 3, pp. 1061–1071, 1973.
[7] S. Valette, J. Lizet, P. Mottier, J. P. Jadot, P. Gidon, and S. Renard, "Integrated-optical circuits achieved by planar technology on silicon substrates: Application to the optical spectrum analyzer," *Inst. Elect. Eng. Proc.*, vol. 131, no. 5, pt. H, pp. 325–331, 1984.
[8] C. Gorecki, F. Chollet, E. Bonnotte, and H. Kawakatsu, "Silicon-based integrated interferometer with phase modulation driven by surface acoustic waves," *Opt. Lett.*, vol. 22, no. 23, pp. 1784–1786, 1979.
[9] D. A. Pinnow, "Guide lines for the selection of acousto-optic material," *IEEE J. Quantum Electron.*, vol. QE-6, no. 4, pp. 223–238, 1970.
[10] W. R. Smith, H. M. Gerard, J. H. Collins, T. M. Reeder, and H. J. Shaw, "Analysis of interdigital surface wave transducers by equivalent circuit model," *IEEE Trans. Microwave Theory Tech.*, vol. MTT-17, pp. 856–864, Nov. 1969.
[11] G. S. Kino and R. S. Wagers, "Theory of interdigital couplers on non-piezoelectric substrates," *J. Appl. Phys.*, vol. 44, no. 4, pp. 1480–1488, 1973.
[12] C. Gorecki, T. Hervé, E. Bonnotte, F. Grimbert, S. Bayat, H. Kawakatsu, and H. Toshiyoshi, "An optical sensor on silicon substrate and application for the *in situ* measurement of a fluorescent marker in small bronchia," U.S. patent 09 023 514, Feb. 13, 1998.

E. Bonnotte, photograph and biography not available at the time of publication.

Christophe Gorecki received the M.Sc. and Ph.D. degrees in optics from the University of Besançon, France, in 1979 and 1983, respectively.

In 1983, he joined the French Civil Aviation Organisation, Paris, France, as an Optical Scientist. In 1984, he joined Laboratoire d'Optique P.M. Duffieux, University of Besançon as CNRS Senior Researcher. His research interests include optical inspection of micro- and nanoscale measurements, applications of image processing techniques in optical metrology, and optical pattern recognition methods. From November 1995 to 1998, he was with the University of Tokyo, Tokyo, Japan, where he was engaged in research and development of optical MOEMS and silicon-based interferometric sensors. He has more than 70 technical papers to his credit.

Dr. Gorecki has been a reviewer for several international journals and has organized and chaired various conferences (Europto/SPIE/CLEO). From 1992 to 1995, he served as National Secretary of the French Society of Optics (SFO). He is a fellow of SPIE.

Hiroshi Toshiyoshi, for a photograph and biography, see this issue, p. 24.

H. Kawakatsu, photograph and biography not available at the time of publication.

H. Fujita, photograph and biography not available at the time of publication.

Kerstin Wörhoff, photograph and biography not available at the time of publication.

K. Hashimoto, photograph and biography not available at the time of publication.